A Dynamic Bidirectional Coupled Surface Flow Model for Flood Inundation Simulation

Chunbo Jiang[1], Qi Zhou[1], Wangyang Yu[1,2] , Chen Yang[3] and Binliang Lin[1]

[1]State Key Laboratory of Hydroscience and Engineering, Department of Hydraulic Engineering, Tsinghua University, Beijing, 100084, China
[2]China Institute of Water Resources and Hydropower Research, Beijing, 100038, China
[3]School of Water Conservancy, North China University of Water Resources and Electric Power, Zhengzhou, 450046, China

Correspondence to: Wangyang Yu (sea198719@126.com)

Abstract. As one of the main natural disasters, flood disaster poses a great threat to township development and property security. Numerous hydrological models and hydrodynamic models have been developed and implemented for flood simulation, risk prediction and inundation assessment. In this study, a dynamic bidirectional coupled hydrologic-hydrodynamic model (DBCM) is developed to simulate and evaluate flood inundation impacts. Based on characteristic theory, as one key feature of DBCM, the proposed method is able to dynamically adapt and alternate the boundary between hydrologic model and hydrodynamic model according to the local flow condition. The proposed model accounts both mass and momentum transfer on the coupling boundary which only mass transfer is considered in existing unidirectional coupling model (UCM) and bidirectional coupled model (BCM). Several benchmark tests were used to validate the performance of DBCM, and the results show good agreement with analytical solution as well as experiments results obtained from reference study. The DBCM effectively reproduces flood propagation process and accounts for surface flow interaction between non-inundation region and inundation region. And then, the DBCM was implemented to a typical mountainous river basin – Helin town located in Chongqing City. The simulation results show its capability for conducting flood simulation which can support flood risk early warning and future management.

1 Introduction

Over the past decades, flood events occurred frequently as one of the most devastating natural hazards which impact millions of people across the world, as a result of global warming, population growth, rapid urbanization and climate change (Zhu et al., 2016). Between 1998 and 2016, economic loss due to flood induced disasters has reached millions of yuan in China (Osti, 2017). Thus, prediction and early warning of flood events play a rather important role in the flood risk assessment and management as well as urban design and policy-making.

With the advances in numerical computation and information technology, a large number of studies have been carried out to investigate the hydrologic process and to assess flood risk. Numerous hydrologic models and hydrodynamic models have been proposed to deal with these related problems (Li et al., 2016; Leandro et al., 2014; Li et al., 2013; Singh et al., 2015; Yu

and Duan, 2014; Yu and Duan, 2014). The purpose of the hydrologic model is to assess the water cycle between and within atmosphere, surface and soil over a wide range of space and time scales involving most of the hydrological processes, e.g. precipitation, evaporation, infiltration, etc. Both lumped and distributed hydrologic model are commonly used in real practice related to flood simulation and water management (Singh and Woolhiser, 2002). Whereas, hydrodynamic model solves the two-dimensional mass and momentum equations with full description of the water flow in the study domain (Yu and Duan, 2014; Patro et al., 2009; Singh et al., 2015), such as the water depth, flow velocity, flow duration, etc. However, when conducting the hydrodynamic simulation, initial and boundary conditions datasets need to be prepared ahead, and the accuracy of the datasets impacts the accuracy of the final results obtained from hydrodynamic models.

Recently, much of efforts have been done on the coupling between hydrologic model and hydrodynamic model to take full advantages of both models. These models can be classified into: unidirectional coupling model (UCM) (Montanari et al., 2009; Choi and Mantilla, 2015) and bidirectional coupling model(BCM) (Yu and Duan, 2014; Yu and Duan, 2017; Thompson, 2004; Zhu et al., 2016). In terms of the widely implemented UCM, the hydrologic model is used on the first stage and the results obtained feed the hydrodynamic model as boundary conditions subsequently. Thus, the flow information is transferred in one-way manner from the hydrologic model to the hydrodynamic model. This makes the UCM easy to conduct in real practice. (McMillan and Brasington, 2008) developed a coupled precipitation-runoff hydrological model with 1D dynamic wave model being used to assess the flood inundation for several flood return periods. Other researchers (Choi and Mantilla, 2015; Grimaldi et al., 2013; Montanari et al., 2009) adopted similar coupling methods to investigate flood risks. Many advanced opens-source and commercial modelling packages (SWAT(Liu et al., 2015), HEC-HMS(Hdeib et al., 2018), DHI MIKE(Rayburg and Thoms, 2009), etc.), can be used into UCM simulation.

However, for the cascade coupling manner and one-way flow information transfer, the UCM cannot make a full description of water movements on the coupling boundary which are always involved with each other. For example, under some specific conditions, flow information from hydrodynamic model may affect the surface runoff yield in hydrologic model(Lerat et al., 2012) and in this case, the flood risk may be underestimated. During a real flood event, the rainfall-runoff production is time dependent and spatial varied among the study basin. BCM is one possible solution for this problem, coupling the hydrologic model with the hydrodynamic model and using rainfall, climate condition, soil distribution and other GIS information as input data. In line with this objective, various techniques have been proposed, ranging from simple approach through changing boundary conditions, such as point source or lateral flow conditions (Bouilloud et al., 2010), to relatively complicate models, such as using the simplified 2-D shallow water equations to simulate overland flow instead of traditional hydrologic model (Viero et al., 2014). The coupled MIKE SHE/MIKE 11 modelling system (Thompson, 2004; Thompson et al., 2004) is one kind of BCM that the discharge can exchange within hydrodynamic and hydrologic models at pre-defined river links. The flow velocity is computed based on water level gradient between MIKE SHE and MIKE 11, and the calculated flow be treated as lateral flow when solving the momentum equation of the hydrodynamic model. And after updating the flow direction, the discharge fed back to the hydrodynamic model in the next time step. Through this approach, the present water level of the

hydrologic model and hydrodynamic model have been used in velocity calculation on the mutual boundary (Bravo et al., 2012; Laganier et al., 2014).

The existing coupling methods, either UCM or BCM, still have some limitations for the flood simulation and prediction. On the one hand, the location of the coupling boundary, where flow information exchange between these two models, is predetermined. Generally, in this paper, model domain areas for hydrological model and hydrodynamic model are defined with non-inundation area and inundation area respectively. The non-inundation and inundation areas are time-dependent according to the local flow conditions. However, a pre-specified coupling boundary leads to the bargain of cost and benefit between simulation efficiency and resources. A very large inundation region will cost more computing resources and reduce efficiency, while a very small inundation region may lead to the flood area being located beyond the pre-set boundary. Thus, the size of domain is one key issue in coupling models. On the other hand, the discharge through the coupling boundary need to consider the flow information of both models. However, the UCM run the hydrodynamic model using the hydrologic model output as the inflow boundary, and the hydrologic model does not assess the feedback effect from the hydrodynamic model, which has been taken into account by BCM. The existing BCM considers the water volume exchange between two models without precise consideration of local velocity information. Taking the MIKE SHE/MIKE 11 coupling model as an example, the velocity of a local grid on coupling boundary is temporal calculated based on flow depth difference between the two models, and the obtained temporal velocity is used to solve momentum equations in hydrodynamic model. This approach is adequate conduct, while the temporal velocity still does not take their own original velocity of both models into consideration which limits its application to 1D flow. Thus, further studies are necessary for general implementation, such as 2D flow or other complicate flow cases. In order to reach the goal of dynamic coupling and keep mass and momentum conservation, the flow states from both hydrologic and hydrodynamic models on the coupling boundary should be taken into account which means the grid-self flow depth and velocity cannot be discarded. Besides, special focus should be paid to the boundary dynamic change and subsequent flow states after the determination of discharge variation.

The aim of this study is to develop a dynamic bidirectional coupling hydrologic-hydrodynamic model (DBCM) capable of realizing the dynamic switching between hydrologic model and hydrodynamic model. The two-dimensional hydrodynamic model and rainfall-runoff hydrologic model are coupled based on the techniques of characteristic wave theory. In comparison to existing approaches, the main advantages of the proposed DBCM are two folds, (1) a dynamic coupling approach of hydro-hydrodynamic model based on characteristic wave theory is developed for the first time, and the flow description of the model is more consistent with the natural flood propagation; (2) the flow information determination based on the theory of characteristic on the coupling boundary is the key point to realize the dynamic switch of the surface flow simulation within both models, and comprehensively consider the local flow state computed by both models.

The methodology of the proposed DBCM is described in section 2. After that, the performance of the proposed model is verified by numerical and physical experiments in Section 3, as well as comparison and discussion with former approaches. In section 4 the DBCM is applied to a real river catchment – Helin town in Chongqing City, and then followed by conclusions.

2 Methodology

The DBCM model comprise a hydrologic model which includes three sub-models (rainfall, infiltration and runoff routing) and a hydrodynamic model which solves 2D shallow water equations used to simulate channel and overland flow. Both models are solved simultaneously within each time step, and the mass and momentum transfer on the coupling boundary are determined based on the characteristic wave propagation theory which is commonly employed in solving Riemann problems (Toro, 2001).

2.1 Runoff generation

The hydrologic model used in this study is a raster-based distributed model. The runoff yield of a catchment involves the hydrological processes, e.g. precipitation and infiltration. 2-D diffusion wave equations is used for overland flow modelling.

The precipitation module reads in record datasets from rainfall stations and rainfall intensity in each grid is interpolated using a spatial interpolation function (Thiessen polygon method, Inverse Distance Weighted, etc.). The infiltration module solves the Green-Ampt equation (Rawls et al., 1983), a theoretical formulation obtained based on Darcy formula with a simpler form as follows.

$$f_{\mathrm{p}} = K_s \left(1 + \frac{(\theta_s - \theta_i) S_a}{F_c}\right) , \quad (1)$$

where f_p is the infiltration rate($\mathrm{mm\ h^{-1}}$), K_s is the hydraulic conductivity($\mathrm{mm\ h^{-1}}$), S_a is the average effective suction of the wetting front (mm), θ_s and θ_i are saturated and initial soil moisture content respectively (%), F_c is the cumulative infiltration (mm). According to the relationship between infiltration rate, soil moisture content and rainfall intensity, this formula can reflect runoff yield conditions under whether saturated storage or excess infiltration, and it has been widely verified and works well.

Surface flow routing models can be divided into conceptual model and physical model. The conceptual model, such as Soil Conservation Service(SCS) formulation (Rallison and Miller, 1982) ,an empirical model for estimating the amounts of runoff under varying land use and soil, and unit line formulation, commonly output the runoff hydrographs at control section, but it is not capable of providing detailed information about the water movement over the entire basin. Moreover, the location of the control section and computing grid cannot be changed once determined. The mesh generation principle of the conceptual hydrologic model is not consistent with that of the hydrodynamic model. Therefore, the conceptual hydrologic and hydrodynamic models cannot be processed using the same computational grid. Hence the conceptual hydrologic model and hydrodynamic model can only be solved sequentially and independently. Nevertheless, the governing equations of the process based hydrologic model often take advantage of the simplified forms of hydrodynamic model (kinematic wave model (Borah and Bera, 2000), diffusion wave model (Leandro et al., 2014; Downer et al., 2002), etc.) to simulate the flow routing process.

2.2 Diffusion wave approach

The diffusion wave equations (Bates and De Roo, 2000) are used to determine the runoff routing, which are composed of mass conservation equation and momentum equations:

$$\frac{\partial h}{\partial t} + \frac{\partial q_x}{\partial x} + \frac{\partial q_y}{\partial y} = Q_m, \tag{2}$$

$$Q_x = \frac{A_x R_x^{0.67} S_x^{0.5}}{n}, \tag{3}$$

$$Q_y = \frac{A_y R_y^{0.67} S_y^{0.5}}{n}, \tag{4}$$

where q_x, q_y are unit discharges along the x and y directions($m^2\ s^{-1}$), h is water depth(m), Q_m equals to rainfall rate minus infiltration rate ($m\ s^{-1}$), Q_x, Q_y are flow rate in the direction of x and y ($m^3\ s^{-1}$), respectively, A is flow area (m^2), R is hydraulic radius (m), S is water level gradient, and n is roughness coefficient.

Since the effect of acceleration and inertial terms of water flow on the urban surface is not obvious compared to gravitational and frictional terms (Chen et al., 2012; Hsu et al., 2000), the time dependent terms in the original momentum equations are omitted, thus two diffusive wave equations are obtained. The numerical scheme can be found in the JFLOW model (Bradbrook et al., 2004; Yu and Lane, 2006). The diffusive wave model does not compute the flux term in the momentum equations. Velocity entirely depends on the local water level gradient and roughness, and water depth relates to discharge from the neighbour grid. The possible flow is up to two of the adjacent cells at each time step (see Fig.01a):

$$Q_i = \frac{w h^{5/3} S_i}{n\left(S_i^2 + S_j^2\right)^{1/4}},\ Q_j = \frac{w h^{5/3} S_j}{n\left(S_i^2 + S_j^2\right)^{1/4}}, \tag{5}$$

where

$$S_i = \frac{\eta_{i,j} - \eta_{i\pm1,j}}{w}, S_j = \frac{\eta_{i,j} - \eta_{i,j\pm1}}{w},$$

$$h_i = \eta_{i,j} - \max\left(z_{i,j}, z_{i\pm1,j}\right), h_j = \eta_{i,j} - \max\left(z_{i,j}, z_{i,j\pm1}\right),$$

$$h = \frac{\mathrm{h_i} S_i^2 + h_j S_j^2}{S_i^2 + S_j^2}, \tag{6}$$

where w is the width of the cell(m), S_i, S_j are water level slope in the orthogonal direction of i and j, respectively, h_i, h_j are effective depth in orthogonal direction of i and j, respectively, $\eta_{i,j}$ and $z_{i,j}$ are the water surface level and ground elevation(m), respectively, and h is the effective depth. The depth definition is shown as Fig.1. The change of water depth in each of the cells is then calculated using the following equation:

$$\Delta h = \frac{\left(\sum Q_{in\ i,j} - \sum Q_{out\ i,j} - Q_m\right)\Delta t}{w}, \tag{7}$$

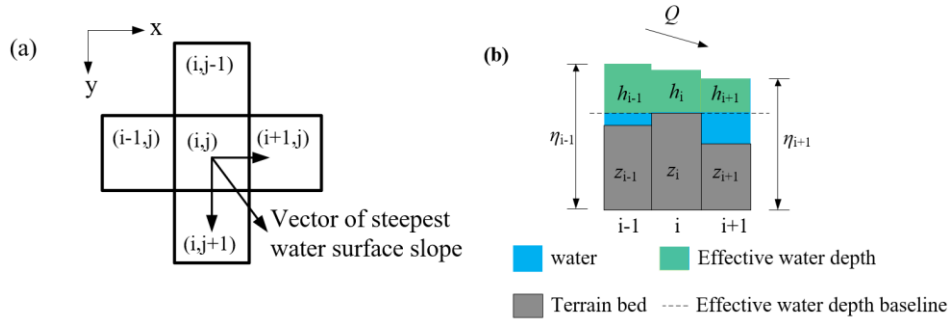

Figure 1 typical grid and water depth definition

2.3 Hydrodynamic model

2D shallow water equations are the most widely used hydrodynamic model in inundation simulation (Bradbrook, 2006; Yu and Duan, 2014; Yu and Duan, 2017). Neglecting the Coriolis force term, wind resistance term and viscosity term, the equations are composed of the continuity equation

$$\frac{\partial h}{\partial t}+\frac{\partial hu}{\partial x}+\frac{\partial hv}{\partial y}=Q_m\,, \tag{8}$$

and the momentum equations

$$\frac{\partial hu}{\partial t}+\frac{\partial}{\partial x}\left(hu^2+\frac{1}{2}gh^2\right)+\frac{\partial}{\partial y}(huv)=-gh\frac{\partial z}{\partial x}-C^2u\sqrt{u^2+v^2}\,, \tag{9}$$

$$\frac{\partial hv}{\partial t}+\frac{\partial}{\partial x}(huv)+\frac{\partial}{\partial y}\left(hv^2+\frac{1}{2}gh^2\right)=-gh\frac{\partial z}{\partial y}-C^2v\sqrt{u^2+v^2}\,, \tag{10}$$

where u, v are velocities along the x and y direction($\mathrm{m\ s^{-1}}$), respectively, h is water depth(m), g is gravity acceleration ($\mathrm{m\ s^{-2}}$), z is bottom elevation(m), C is Chezy coefficient representing roughness, Q_m is the source term which equals to rainfall rate minus infiltration rate ($\mathrm{m\ s^{-1}}$).

These equations are solved using the finite volume method similar to TELEMAC (Ata et al., 2013). And the convection flux on grid faces is calculated using the HLL scheme with WAF approach (Toro, 2001).

$$\begin{cases} F^{hll}=F_L & S_L\geq 0 \\ F^{hll}=\frac{S_RF_L-S_LF_R+S_LS_R(U_R-U_L)}{S_R-S_L} & S_L\leq 0\leq S_R\,, \\ F^{hll}=F_R & S_R\leq 0 \end{cases} \tag{11}$$

$$S_L=U_L-\sqrt{gh_L}, S_R=U_R+\sqrt{gh_R}\,,$$

where U_L, U_R, h_L, h_R are the components of the left and right Riemann states for a local Riemann problem, and S_L, S_R are estimates of the speeds of the left and right waves. F^{hll} is the fluxes in the middle region. Based on this flux, the WAF method guarantees a second order accuracy in time and space is proposed:

$$F_{i+\frac{1}{2}}=\sum_{k=1}^{N+1}\beta_kF_{i+\frac{1}{2}}^{(k)}$$

$$\beta_k = \frac{1}{2}(c_k - c_{k-1}), c_k = \frac{\Delta t S_k}{\Delta x}, c_0 = -1 \; and \; c_{N+1} = 1\,, \tag{12}$$

where $F_{i+\frac{1}{2}}^{(k)} = F\left(U^{(k)}\right)$, N is the number of waves in the solution of the Riemann problem, and β corresponds to the differences between the Courant numbers c_k of successive wave speeds S_k.

The topography term on the right hand side of equation (9) and (10) is calculated by the hydrostatic reconstruction scheme:

$$-gh\frac{\partial z}{\partial x} = \nabla\frac{gh^2}{2} = \frac{g}{2}\frac{\Delta t}{\Delta x}[(h_i^R)^2 - (h_i^L)^2]\,, \tag{13}$$

$$\begin{cases} h_i^R = max[0.0, h_i + z_i - max(z_i, z_{i+1})] \\ h_i^L = max[0.0, h_i + z_i - max(z_{i-1}, z_i)] \end{cases},$$

The friction term is computed by a semi-implicit scheme to ensure numerical stability (Liang et al., 2007):

$$(hu)^{n+1} = \frac{(hu)^n}{1+\Delta t\left(\frac{g\sqrt{(hu)^2+(hv)^2}}{h^2C^2}\right)^n}\,, \tag{14}$$

The time step is determined by CFL condition as following.

$$\Delta \mathrm{t} = \mathrm{C_r}\min\left(\frac{\Delta x_i}{|u_i|+\sqrt{gh_i}}, \frac{\Delta y_i}{|v_i|+\sqrt{gh_i}}\right), \tag{15}$$

Where $\mathrm{C_r}$ is Courant number, limited by $0 < \mathrm{C_r} \leq 1$ for simulation stability, a typical value of 0.9 is used for the following simulation cases. More details of the numerical schemes can be referred to (Ata et al., 2013).

2.4 Coupling approach

The computation domain in DBCM is divided into non-inundation regions and inundation regions, and the diffusion wave equation(DWE) is solved in non-inundation region with small water depth while the hydrodynamic model(SWE) is applied in inundation regions with high water depth and discharge. The model for a specific grid is determined based on its own and neighbouring flow state. The boundary between the non-inundation regions and inundation regions forms the dynamic coupling boundary which is time dependent. Besides, special treatment on discharge through the coupling boundary need to be taken based on the local flow state using the characteristic theory.

The flow status always changes time to time, and the model applied also alters based on given criterion. This leads to the changes of coupling boundary position accordingly. As shown in Fig.2, with the increasing of rain intensity, the inundation region expands as a consequence of the gradually accumulating of surface water volume from upstream regions. The position of the in-flow boundary, flow path and discharge change subsequently. The coupling models proposed by other researchers, either UCM or BCM, consider less of this phenomenon.

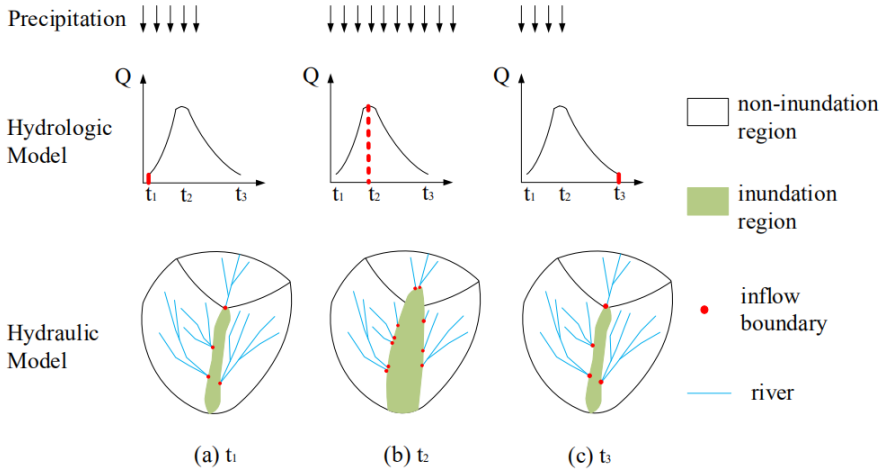

Figure 2. Schematic diagram of DBCM

Figure 3 shows a detailed process of flow state change on both sides of the coupling boundary. Fig.3a shows the case of the flow on slope flows to the channel. The discharge on the coupling boundary equals to the upstream discharge and not affected by the downstream flow, which means the local discharge is completely determined by DWE. After the water depth is updated, the location of the coupling boundary point O is moved to point A according to the comparison of its water depth to the water depth threshold. Moreover, in the inundation region the flow may move from downstream to upstream, as shown in Fig.3b. The discharge and water depth on the coupling boundary should be determined by the flow on both sides. In this case, the coupling boundary location moves to point B due to inundation area expanding.

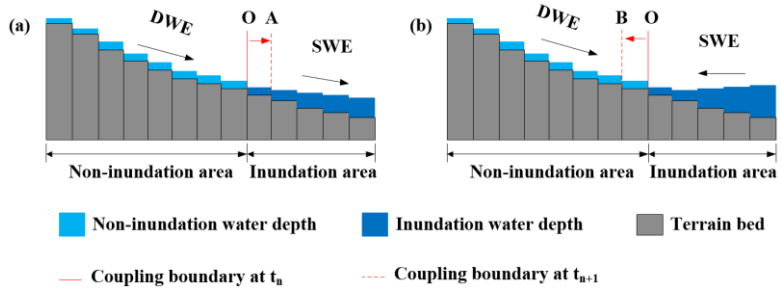

Figure 3. Flow state change and position of the coupling boundary

In previous studies by other researchers, the discharge on the coupling boundary may be computed directly through the hydrologic model, using empirical formulae, or by interpolation approaches according to the water level or velocity gradient on both sides. Such methods may still fail to provide an overall understanding of the flow regime status of the combined hydrologic and hydrodynamic model. The DBCM is conducted as following procedures on the coupling boundary: the flow state is obtained by both the hydrologic and hydrodynamic models in their local grids, then the discharge through the coupling boundary is computed and the entire water depth is updated according to the water volume variation. After that, the location of the coupling boundary is updated and the area of non-inundation region and inundation region are remapped. The key issue

of DBCM is to establish a reasonable approach to determine the discharge on the coupling boundary, which need to integrate the effect of current flow state obtained by both models on both sides of the coupling boundary.

According to Godunov theory (Godunov, 1959), the solution of convective flux implementing the finite volume method can be considered as a local Riemann problem. The discontinuity characteristics speed between each grids represent the propagation of local fluid variables in time and space, as shown in Fig.4. When the characteristic speeds are all positive, the flux depends entirely on the left-side flow state, and vice versa. However, when the characteristic speeds have a negative value and a positive value, both the current flow state in the two grids must be taken into consideration. Applying this theory to DBCM, the computational scheme at the boundary can be specified. It is known that the hydrologic model only transfers water mass, while the hydrodynamic model transfers both water mass and momentum. More details of different coupling cases are shown Fig.5.

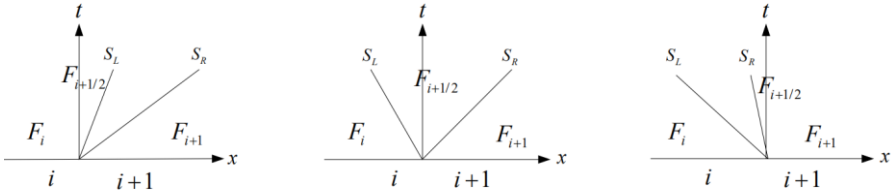

Figure 4. Direction of Characteristic wave

For first case in Fig.5a, the hydrologic and hydrodynamic models are calculated independently, corresponding to the situation that positive bed slopes inducing confluence flows into the river, thus only the discharge calculated by the hydrological model passes through the coupling boundary (Fig. 3a). The flow information in grids *k* and *i* is calculated using DWE and grid *j* using SWE, see Fig. 5a. Firstly, slope analysis of DWE is applied uniformly. Obviously the water level gradient between *k* and *i* is smaller than that between grid *i* and grid *j*. According to the calculation results from the DWE, the velocity points to the maximum water level slope (in Fig.1a, flow directs to right). Therefore, the change of water depth in grid *k* has nothing to do with the flow state at grid *i*, and the velocity change at grid *k* is analysed by the other grids on the left of grid *k*. The flow information at grid *i* and *j* forms a local Riemann problem and then the characteristic speed is analysed. The velocity at grid *i* is obtained from above analysis, and the velocity at grid *j* is the velocity at current moment. The interface water depths at contact discontinuity are calculated as: $h_i^r = h_i + z_i - \max(z_i, z_j)$, $h_i^l = h_j + z_j - \max(z_i, z_j)$. Thus a pair of characteristic wave at the interface are obtained:

$$S_L = u_i - \sqrt{g h_i^R}, S_R = u_j + \sqrt{g h_j^L}\,, \tag{16}$$

When the characteristic speeds $S_R \geq S_L > 0$, the flux calculation only depends on the flow information at grid *i*, independent of that at grid *j*. The velocity at grid *i* is calculated using the diffusion wave equations and only outflow is allowed. In addition to the water depth change calculated according to the hydrodynamic model at grid *j*, the water volume transferred from grid *i*

should also be added. No convection term in the momentum equation of DWE indicates no momentum transfer at the discontinuity between grid *i* and grid *j*, and thus the velocity of the two grids does not interact with each other.

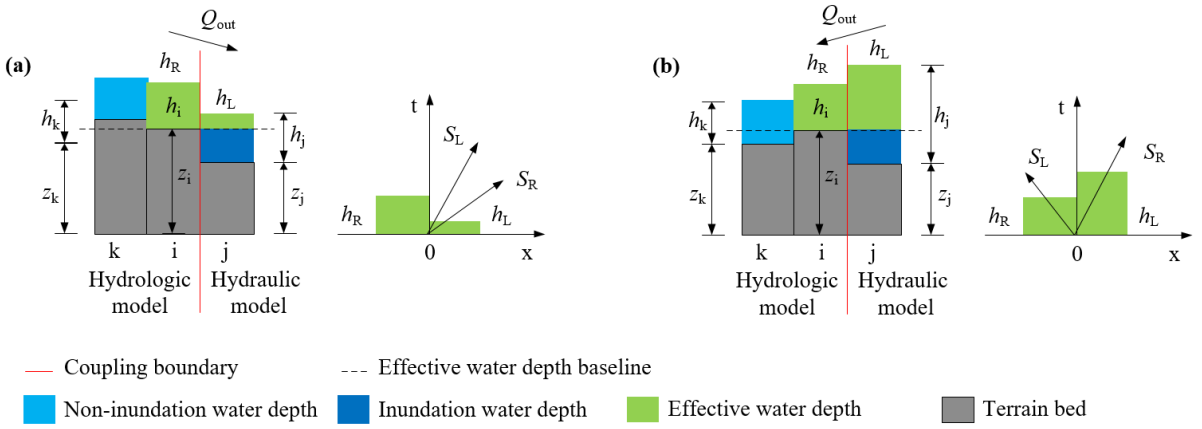

Figure 5. Coupling condition A: discharge on coupling boundary depends on hydrologic model

For the second case in Fig.5b, the hydrological model and hydrodynamic model are calculated together, corresponding to the situation that inundation area expanding (Fig.3b). As shown in Fig. 5b, the water depth in grid *k* and grid *i* are small, and the hydrologic model is applied. While grid *j* has a deeper water depth and smaller elevation, the hydrodynamic model is applied. In this case, the velocity direction is form grid *i* to grid *k*. The characteristic wave analysis at the interface of grid *i* and grid *j* reveals that $S_R > 0 > S_L$, which means that the momentum at grid *j* can be transferred to grid *i*. Grid *i* is involved in the computational domain of the hydrodynamic model. The water depth increment at grid *i* needs to deduct the current discharge output to grid *k* and the flow rate obtained by solving the hydrodynamic equation with the flow state at grid *j*. The velocity increment at grid *i* is obtained by solving the hydrodynamic equation with the flow state at grid j based on current velocity. Then the flow state at grid *i* is updated. And coupling boundary position may change when water depth varies.

The slope gradient analysis and characteristic wave analysis are key issues of the computational theory for solving DWE and SWE respectively. The key point to couple these two approaches is to successfully address the connection on the coupling boundary. As discussed above, in existing research only one governing equation is solved throughout the computational domain, but hardly considering the interaction between two kinds of governing equations and resized the area of different computational domain. A reasonable and implementable approach coupling the solution procedure of DWE and SWE is the precondition for establishing DBCM. In this study, the slope gradient analysis is performed to determine the current calculated velocity together with current depth, and the characteristic wave analysis is conducted on coupling boundary as long as velocity and depth have been provided, no matter it is calculated from hydrologic or hydrodynamic model. Then, flow information exchange on coupling boundary is determined according to the characteristic speed which reflect the propagation of flow state in time and space. This method integrates hydrologic model and hydrodynamic model into a comprehensive system by means of joining the two core steps of slope gradient analysis and characteristic wave analysis together.

In the proposed DBCM, the coupling boundary position will not keep fixed in advance throughout the calculation process. The location where the runoff enters the inundation region varies dynamically, and the flood level can also submerge the original inflow points and regenerate new coupling boundaries. Such alternation mechanism is close to natural flow processes. The characteristic wave theory is used to determine the mass and momentum exchange through the coupling boundary. Compared to the "cascade" operation in UCM, the present DBCM solves DWE and SWE simultaneously. When non-inundation regions get larger, the flow movement is mainly obtained by utilizing DWE. Whereas, when the inundation regions extend, the computational domain is given priority to SWE.

3 Model validation

The numerical model results from DBCM are compared with analytical solutions, experimental data, and results obtained from existing numerical models. Considering the complexity of the numerical model schemes used in the hydrologic and hydrodynamic models, the hydrodynamic model performance will be validated in the first stage, and then the performance of DBCM will be verified using a V shaped catchment. As described in 2.2, the numerical schemes of the hydrodynamic model (referred to HM2D in the following section) used in this study have second order accuracy in both time and space.

3.1 Oblique hydraulic jump

The oblique hydraulic jump example is a special flow pattern, with an analytical solution being available in open channel flows, which is often used to verify the capability of the numerical scheme in simulating shock wave formation. When a supercritical flow is deflected by a converging wall at an angle θ, the resulting shockwave forms an oblique hydraulic jump at an angle β, as depicted in Fig. 6. Both the angles of water surface lines behind the shock wave front can be obtained by analytical solution. In this study, the upstream water depth and velocity are set as 1m and 8.57m s^{-1}, and the oblique angle $\theta = 8.95°$. The width and length of channel are 30m and 40m respectively. In these conditions, the exact analytical solutions are downstream water depth $D_A = 1.49984$m, downstream velocity $V_A = 7.95308$ m s^{-1}, and angle $\beta = 30°$ (Rogers et al., 2001) when flow reaches a steady state.

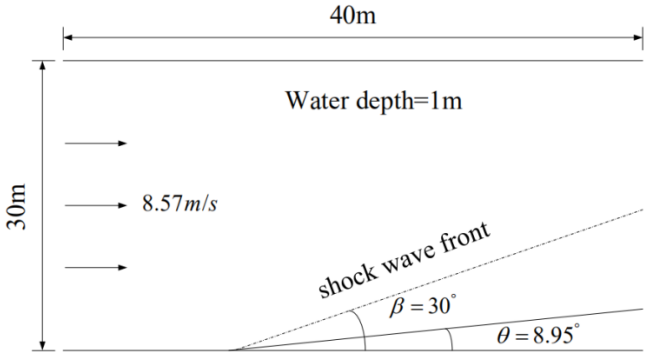

Figure 6. Oblique hydraulic jump: definition sketch

The spatial step size is set as $\Delta x = \Delta y = 0.33$m. The time step is set to dynamic adjustment and total calculating time is 90s. Figure 7 shows a 3-D view water depth results predicted by our model. The oblique jump is sharply captured, and has an angle $\beta \approx 32°$. The average water depth downstream behind the shock front is 1.532m, and the average velocity is 7.86m s^{-1}. The numerical solution is close to the analytical solution, as shown in Table 1. The results of references are also shown below. The output of HM2D and the references, either the water depth or velocity, show good agreement (see Table 1).

Table 1. Comparison between analytical solution and calculation result for oblique jump case

	Angle β	Water Depth(m)	Velocity(m s^{-1})	Depth Error(%)	Velocity Error(%)
Analytical solution	30°	1.49984	7.95308	-	-
HM2D results	32°	1.532	7.86	2.1	1.2
Reference results	30°	1.53	7.9	2.0	0.6

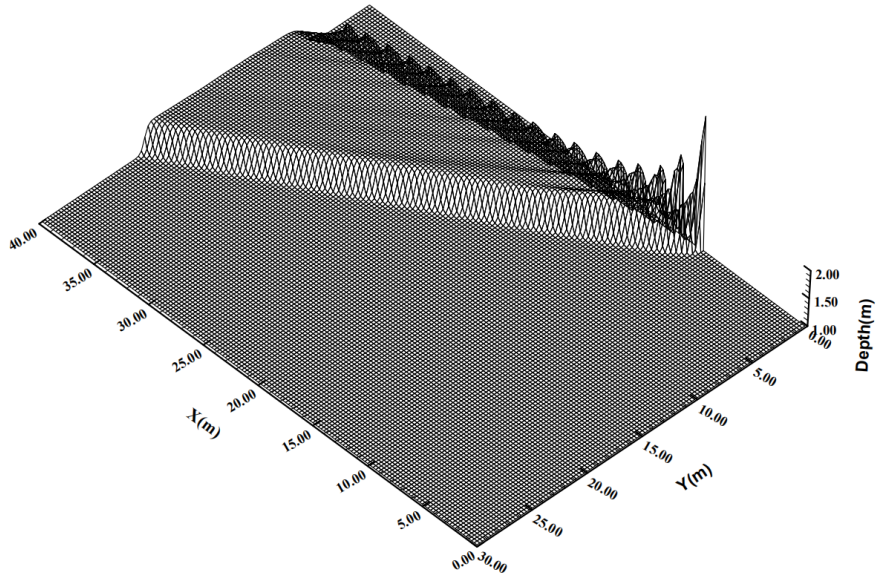

Figure 7. Steady state of water depth of oblique hydraulic jump

3.2 Dam-break over a dry of flood plain

Dam-break is a classic benchmark problem, which is often used to verify the capability of a numerical scheme in dealing with dry-wet boundary, and the physical experimental model is easy to conduct. Thus, it is convenient to collect measured data for comparison with numerical results. An experiment performed by (Fraccarollo and Toro, 1995) was used to validate the DBCM developed in this study. The entire model domain is 3m×2m, which is separated into two areas by a dam at X=1m. Initially, the still water with a depth of 0.64m in the reservoir is surrounded by solid walls, while the downstream area is initially dry.

The boundaries of the downstream floodplain were all open flow. A 0.4m wide section in the middle of the dam was breached instantaneously. The numerical model spatial step is $\Delta x = \Delta y = 0.04$m, and roughness coefficient is $n = 0.01$.

Figure 8 shows the water surface elevation at different times. It can be clearly seen that as the bore wave propagate toward downstream initially. A depression wave travels upstream, which is reflected back by the walls surrounding the reservoir, causing the water surface elevation in the reservoir to oscillate. In Fig.9, a comparison between the measured and computed water level data was made, which shows a good agreement. The results are encouraging and the overall trend is well captured.

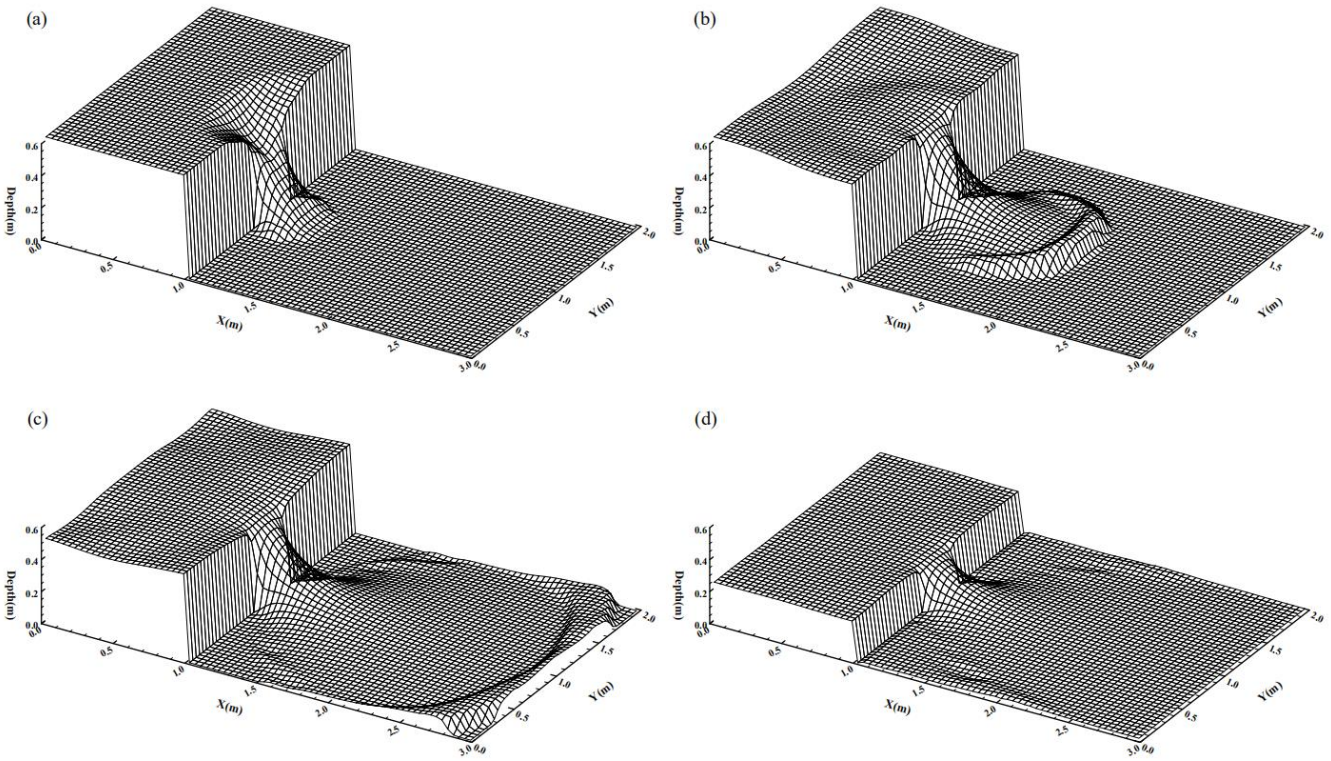

Figure 8. Snapshot of the water elevation for dam-break simulation: a. t=0.1s; b. t=0.5s; c. t=1.1s; d. t=5.0s

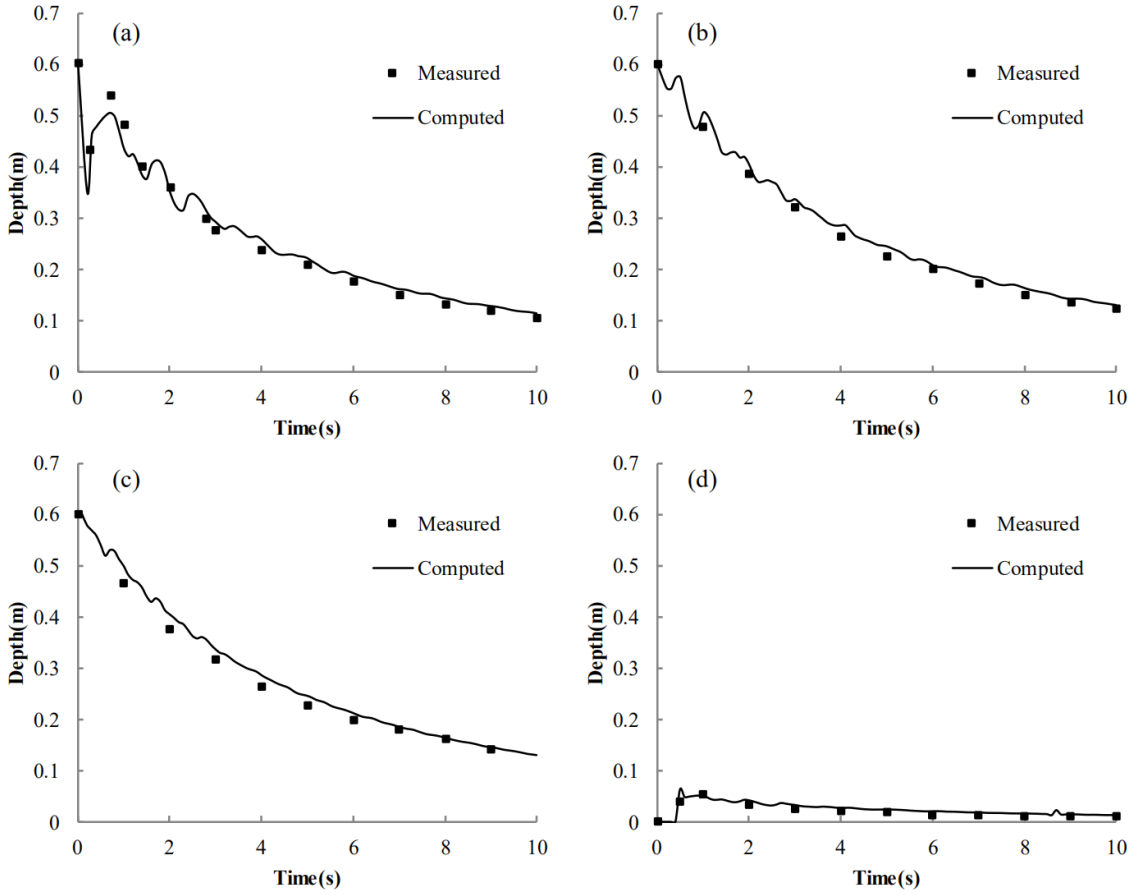

315 **Figure 9. Comparison of water depth variation at four positions: a. x=1m. y=1m; b. x=0.18m, y=1m; c. x=0.48m, y=0.4m; d. x=1.802m, y=1.45m**

3.3 Two-Dimensional surface flow over a tilted V-shaped catchment

A two-dimensional surface flow over a tilted V-shaped catchment is simulated (Di Baldassarre et al., 1996; Panday and Huyakorn, 2004), we aim to verify whether the computational domains of the hydrologic and hydrodynamic models can 320 dynamically switch and compare the difference between the DBCM, UCM and BCM. As shown in Fig.10, the topography of the example is depicted.

The computational domain is symmetrically V-shaped, with a pair of symmetrical hillslopes forming a channel at the central region. The bed slopes are ±0.05 spanwise, and 0.02 streamwise parallel to the channel. The manning coefficient on the hillslope is 0.015 while it is 0.15 in the main channel. The total simulation time is 180min and the constant rainfall intensity is 325 10.8 mm h^{-1} for a duration of 90 min. Fig.10 shows the detailed dimension and related information of the V-shaped catchment.

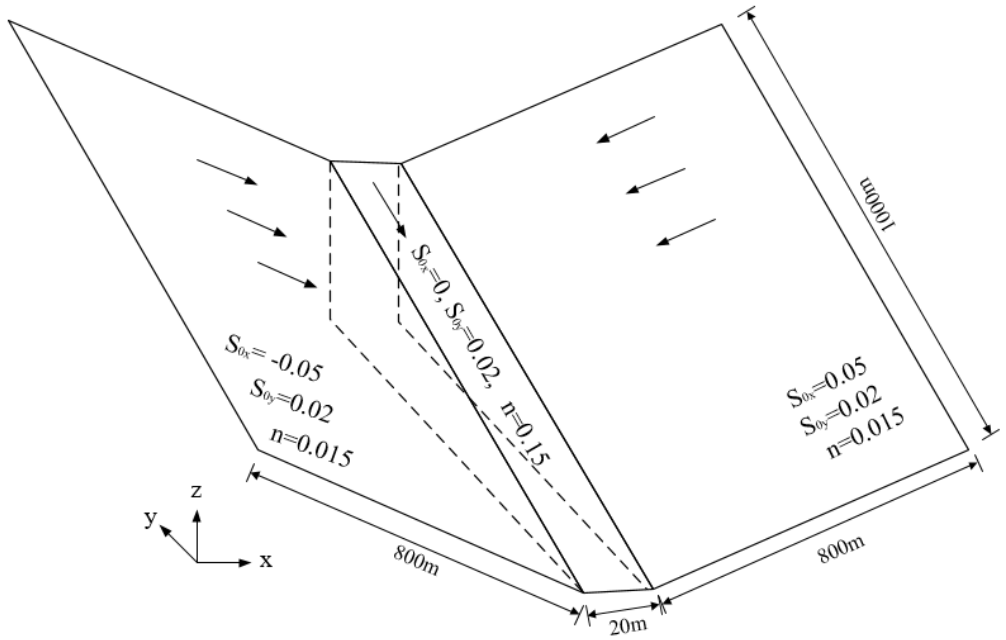

Figure 10. Diagram and dimension of the tilted V-shaped catchment

Considering the hydrodynamic model providing more details to describe the overland flow than the hydrologic model, the HM2D and DBCM under the same rainfall conditions were adopted. The water depth threshold for DBCM to distinguish the hydrological model and the hydrodynamic model is set to 0.005m. When water depth is less than the threshold, the grid is calculated using the hydrological model, and when water depth greater than the threshold the grid is applicable to the hydrodynamic model. Results are compared with reference numerical models developed by (Di Baldassarre et al., 1996; Panday and Huyakorn, 2004; Yu and Duan, 2014).

As shown in Fig.11, the discharge hydrographs obtained by the HM2D and DBCM are compared with other existing models. The discharge hydrographs show good agreement for the peak discharge. The start periods of discharge rising and receding limbs simulated by the HM2D and DBCM are consistent with those predicted by others. However, discrepancies gradually grow, so that both the HM2D and DBCM under-predict the discharge. Despite this disparity, the overall trend of the hydrographs indicates that the accuracy of the proposed models are satisfactory.

Comparing the hydrographs between the HM2D and DBCM, it can be seen that their rising limb and peak discharges are in very good agreement. Consequently, both models adopted the hydrodynamic model to simulate the overland flow. The difference between the HM2D and DBCM gradually emerges at the receding limb due to the switching of applied models. The HM2D simulates water movement using hydrodynamic model (SWE) throughout the computation process, while the DBCM switches from the hydrodynamic model to the hydrologic model (DWE) when the upstream water depth falls below threshold. Since no time partial derivative terms in the hydrologic model, the velocity at the present is a function of the current water level gradient, and is not equal to the velocity at the previous moment plus the flux term. For this reason, when the DBCM

switches from the hydrodynamic model to the hydrologic model, the velocity calculation approach changes accordingly, and the discharge difference between the HM2D and DBCM emerges. Therefore, the outlet flow is slightly larger, but later slightly smaller, in the DBCM, assuring the overall is mass conserved.

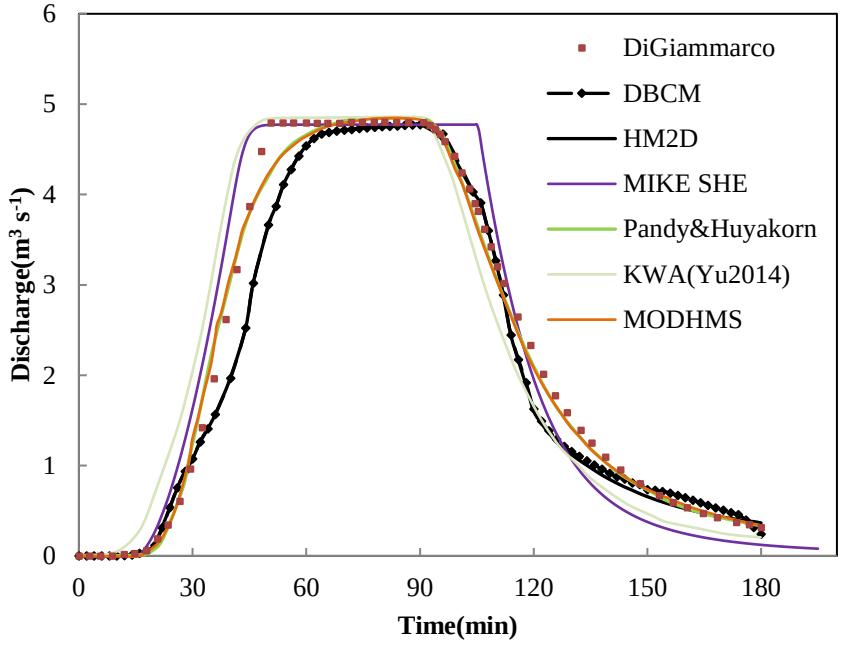

Figure 11. Comparison of discharge hydrographs of the V-shaped catchment

The spatial variability of flow depth, velocity and flux in x,y direction at 90 min and 120min are shown in Fig.12 and Fig.13. The hydrological model and the hydrodynamic model are solved simultaneously in DBCM. The main difference between the governing equations of the hydrologic model and hydrodynamic model is that the flux term is not calculated in the former, meanwhile the latter needs to calculate the convection term. The non-inundation region and inundation region can be determined by whether the flux term is generated during the calculation process. When t=90min, the rain stops, the water depth reach the peak value and the flow information is determined by the hydrodynamic model over the whole domain. At t=120min, the water continues to flow to the outlet and the water near the upstream region decreases, but a small amount of water still exists. No flux is calculated while velocity computation continues. Obviously, a sharp division line separating the domain arises at this moment.

For DBCM, the coupling boundary between DWE and SWE is time dependent. Fig.14 shows the evolvement of the coupling boundary. During the first 90min, rainfall keeps constant among the whole catchment and water depth arises in a short time. As a result, water depth in almost all of the region is larger than the depth threshold and SWE was implemented to most of the simulation domain. However, 90min later, the rainfall stops and no extra water flow into the domain. Then, water depth begins to decrease. Once the depth is lower than the depth threshold, the grid cell use DWE to determine discharge and depth and the coupling boundary shrinks (see Fig.14). The evolution of coupling boundary is consistent with the flux analysis stated above.

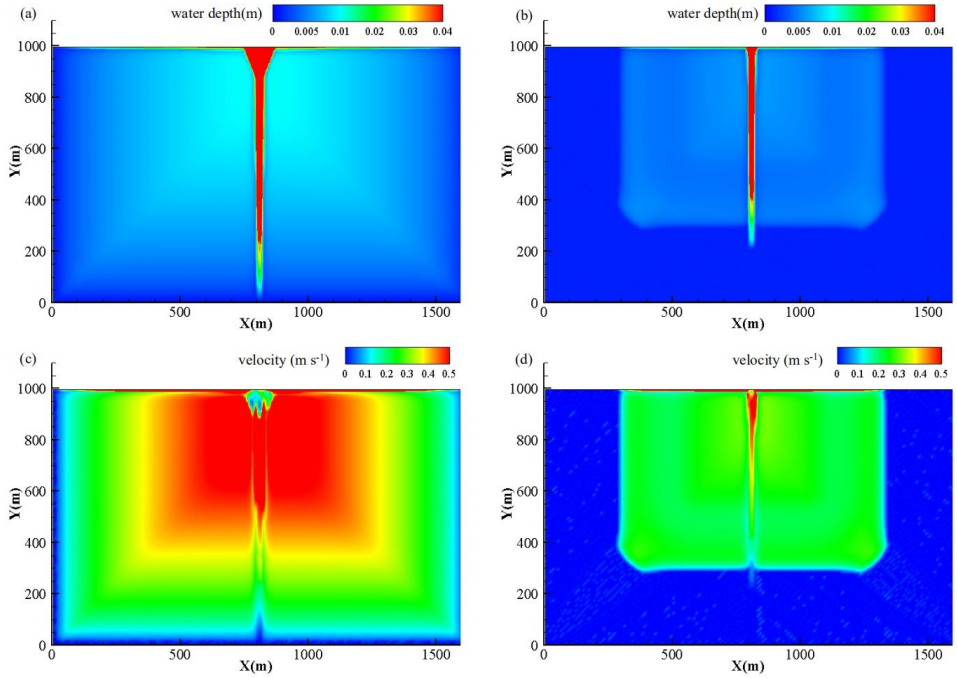

Figure 12. Water depth and velocity distribution at 90min(a and c) and 120min(b and d)

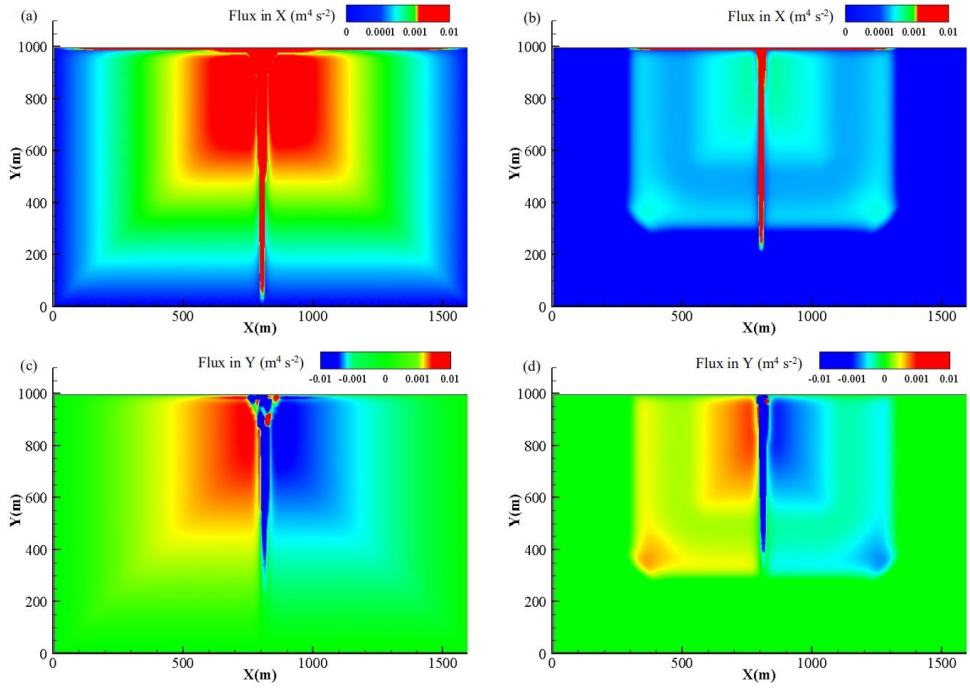

Figure 13. Flux distributions of in X and Y direction at 90min(a and c) and 120min(b and d)

370

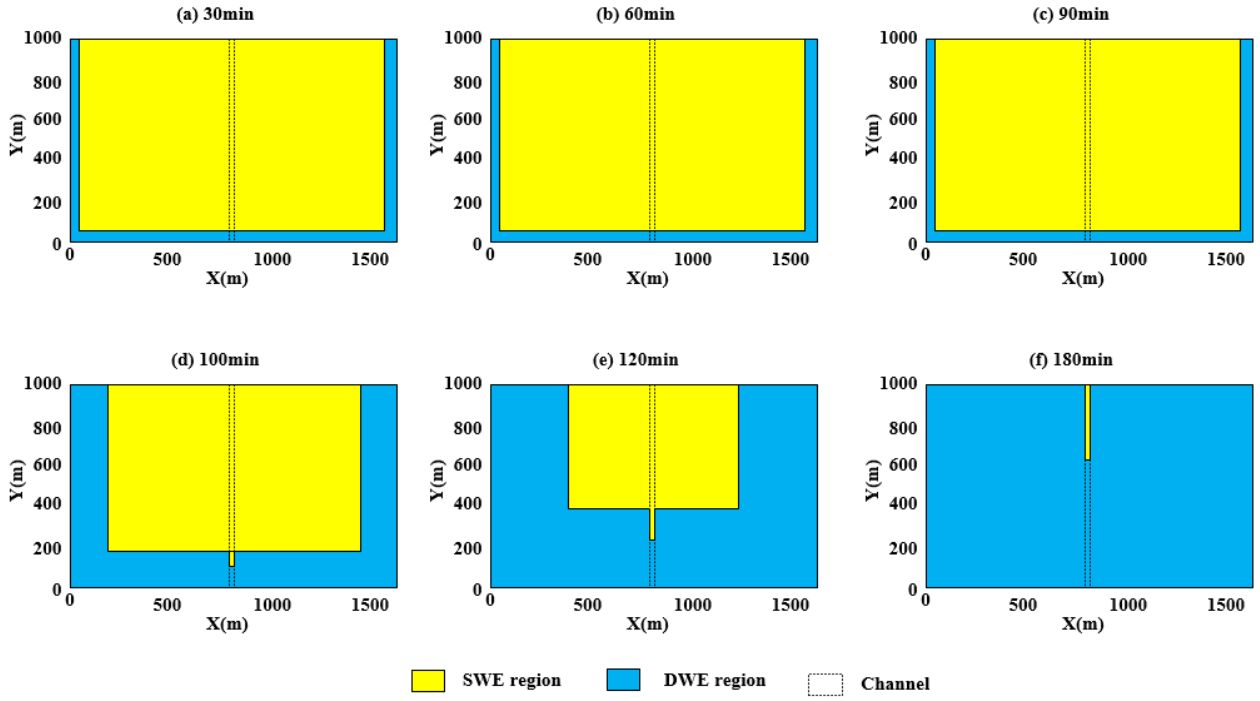

Figure 14. Evolvement of coupling boundary

It is well known that solving SWE needs large number of resource and time. This limits its application, especially for large scale simulation. In terms of this small scale V-shaped catchment, the simulation performance between SWE, DBCM and DWE was conducted. Fig.15 shows the result and the simulation time of SWE was used as the reference (100%). It can be seen that both DBCM and DWE need less simulation time compared to SWE, especially for DWE nearly 15% simulation time saved. Whereas, DBCM alters the SWE and DWE according to the local flow information of each grid. Compared with SWE, the simulation time of DBCM was only a small lower than SWE for the reason that in the early half simulation time in this V-shaped catchment most of the flow information is calculated by SWE as discussed in above section (Fig.14). When implemented to large scale catchment, the simulation time of DBCM would be much less than SWE.

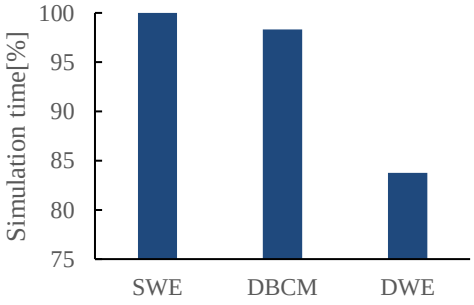

Figure 15. Relative simulation time of different models

Finally, the need for model transformation is discussed. Flood propagation is a phenomenon of high speed movement with drastic change of water depth and velocity. The hydrologic model(DWE, omitting convection term) is insufficient to describe this movement. Fig.16 depicts the rapid change of water depth profile near the outlet in a short time, while the water depth on both sides of hillslopes hardly changed. This leads to strong convective flow near the channel, and the momentum transfer need to be taken into consideration in order to get reasonable simulation results.

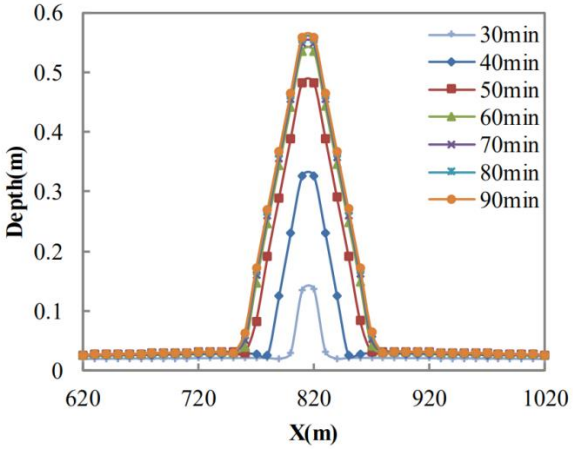

Figure 16. Evaluation of water depth profile at the channel outlet

4 DBCM implemented to a natural watershed

The proposed DBCM was implemented to a natural watershed for flood risk assessment, that is, Helin town of the Longxi River in Chongqing City. The Longxi river basin is located in the eastern region of Chongqing (see Fig.17), which is a first-class tributary of the Yangtze River. The main channel length is about 221km and the basin area is about 3280km^2. The overall terrain gradually goes down from northeast to southwest, consistent with the trend of the main channel. Most of the central and southwest areas are relative flat areas, and the east and west areas are mountainous, a typical topography of a trough sandwiched by two mountains. The average annual rainfall in the basin is 1192.4mm, which is prone to heavy rain in summer, and the flood spreads rapidly to the central district as a consequence of the topographic feature. The selected catchment, Helin town, located in the northeast of the Longxi river basin, was chosen as a case study for investigating the surface flow phenomena using the DBCM. The administrative location and DEM information of Helin town is shown in Fig.17.

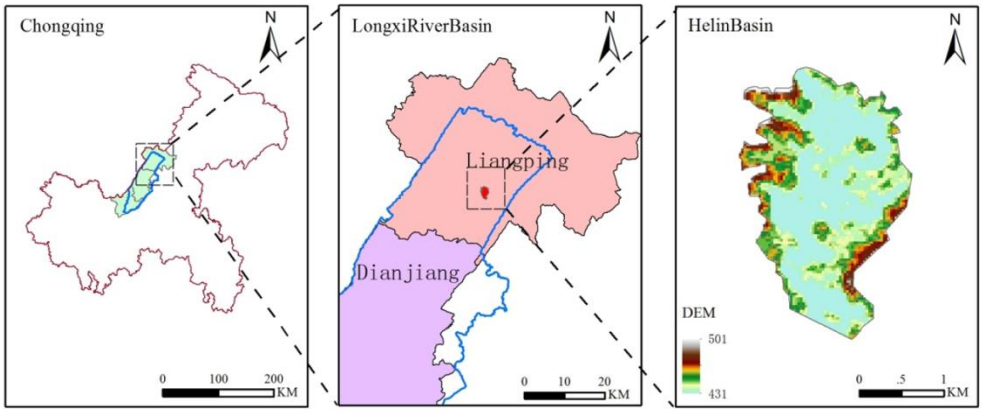

Figure 17. Location of Helin town. Chongqing City(left), Longxi river basin (middle), Helin basin(right)

The river section in Helin basin is a typical mountainous river. The upper part of the river has a steep slope, while the middle and lower reaches are relatively gentle. At present, no flood protection works exist on the river banks along the main channel. The terrain along the river is open plain, and the farmland is widely distributed, resulting in the poor ability to resist flood disasters. Once heavy rainfall occurs and flow overtops the river banks, the residential area and farmland along the river will be inundated. Floods in Helin town are always caused by heavy rainstorm, and the flood season is consistent with the rainstorm season which lasts from April to September. Heavy rainstorms and flood often occur during this period.

The input datasets for DBCM include DEM, LULC(land use and land cover) and soil type as shown in Fig.17 and Fig.18. DEM data were obtained from the GDEMV2 database with a spatial resolution of 30m. The DEM was resampled according to some channel section field survey data to get finer resolution. There are four main kinds of land use in Helin basin: urban, forest, farmland and water. Besides, several soil types with little proportion have been consolidated into the categories with a large ratio. Soil properties determine the infiltration rate, which further affect the surface runoff. The parameters, such as roughness and soil moisture content, are extracted from the public data provided by local administrative sectors. The LULC data are processed by remote sensing interpretation tools using the satellite image. The soil data are processed by SWAT, Soil-Plant-Air-Water (SPAW) model using the Harmonized World Soil Database (HWSD). Then the collected parameters are conformed according to the reference opinions for hydraulic engineering construction provided by local water conservancy department.

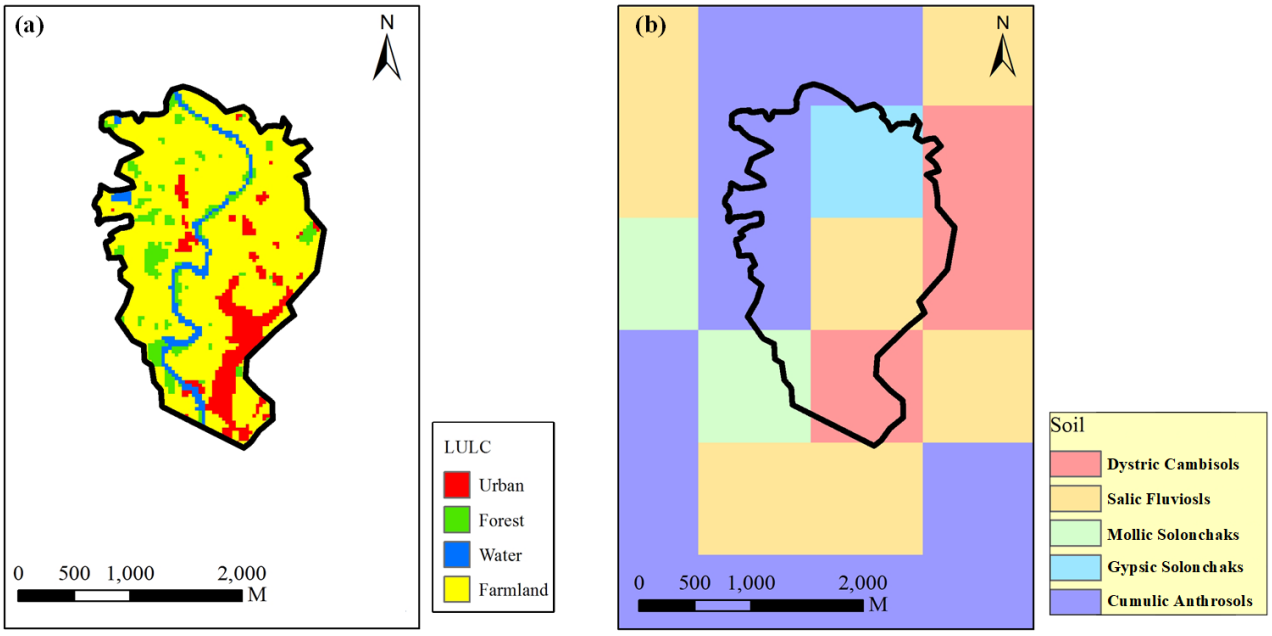

Figure 18. LULC and Soil of Helin basin

The DBCM was applied to simulate the rainfall runoff process in Helin town and the result was compared with a UCM composed of SWAT(as hydrologic model). The SWAT was calibrated by the design storm and hydrographs (flood return period of 1%) in the Helin town outlet. The selected coefficients and parameters of rainfall and flood event are listed in Table 3 and Table 4. The calibration results are shown in Fig.19. It can be seen clearly that the flood process calculated by the SWAT model is very similar to the design flood, with similar flood peak flow and fluctuation process. At the beginning of the simulation, because of the soil infiltration, no surface runoff occurs although the rainfall exists for a short time. Then, when the soil saturated, the discharge curve climbs rapidly which is consistent with the rainfall intensity. The simulation result reflects the storm runoff production process affected by the combined action of rainfall and infiltration. The hydrographs show good agreement with the design flood, demonstrating that results from SWAT are reliable for hydrodynamic model. Once being calibrated, the hydrographs generated by SWAT at different locations were extracted and applied as inflow boundary conditions for hydrodynamic models. Two simulation scenarios were designed, as shown in Table 2.

Table 2. Simulation scenarios

Case	Model	Boundary condition	Descriptions
A	HM2D	Helin outflow as inflow BC	SWE
B	DBCM	Helin inlet flow	Coupling DWE and SWE

Table 3. Rainfall parameters (Cs: coefficient of skewness Cv: coefficient of variation P: flood recurrence period)

Duration (h)	Mean value (mm)	Cv	Cs/Cv	P(%)			
				1	2	5	10
6	81.7	0.5	3.5	**224**	197	162	137
24	112	0.48	3.5	**297**	263	218	183

435

Table 4. Peak discharge at Helin outlet for different flood frequency

P(%)	**1**	2	5	10	20	50
Discharge (m^3 s^{-1})	**2280**	1920	1470	1150	831	433

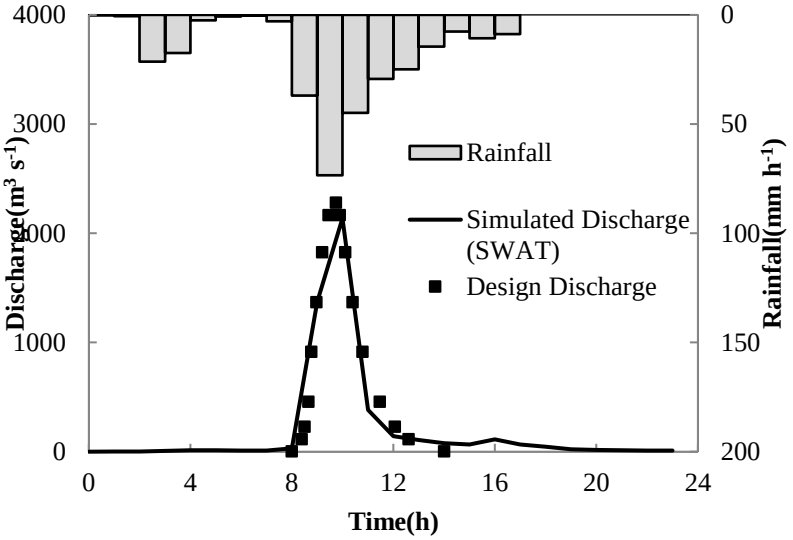

Figure 19. Design rainfall and discharge with simulated flow in Helin basin outlet(1%)

440 The results from Case A and Case B are compared to investigate the capability of the DBCM. Fig.20 depicts the maximum water depth distribution in Case A and Case B. The inundation region has expanded significantly in Case B. Not only the lowland areas, but the hillsides have been inundated. Even though Case A adopted the simulated outlet hydrographs larger than that used in Case B, the runoff failed to inundate the hillside because of topographic obstruction. The red cycle in Fig.20 indicates the urban area. Water depth was extracted for each cases. Due to the lack of measured data, field survey and historical
445 records have to be used as reference data to verify the model outputs. The current river bed conditions are as following: both sides of the river are flat, with a lot of farmland and some villages distributed along the main river. No embankments or bank protection works have been built along the river. All of these problems lead to low flood control capacity in the catchment. As local residents recall, in 2017, the flood covered the middle of the trees along the bank, equivalent to at least 3m water depth. When in terms of the urban area, according to the historic record, the rainstorm in 12 August 1998 caused a flood that local

streets and airports were inundated with water depth of 1.0m and 1.4m respectively. All villages and towns in the Helin town catchment were submerged with water depth exceeding 0.5m on average. In Case B, this phenomenon was simulated that the maximum water depth in urban areas is more than 0.6m, in accord with the historic data. But no water emerged in Case A, although the Helin outlet flow is utilized as inflow discharge, greater than that of Case B, as shown in Fig.21. Referring to local topography, the main reason for this problem is that urban locates in a higher position, between riverbed and hillside, hence the upwelling movement of water in rivers is easily blocked due to local terrain. Nevertheless, urban area will be submerged by uphill surface flow, even though the river flow has been obstructed. Obviously, the computed results of Case B by the DBCM are closer to the practical situation.

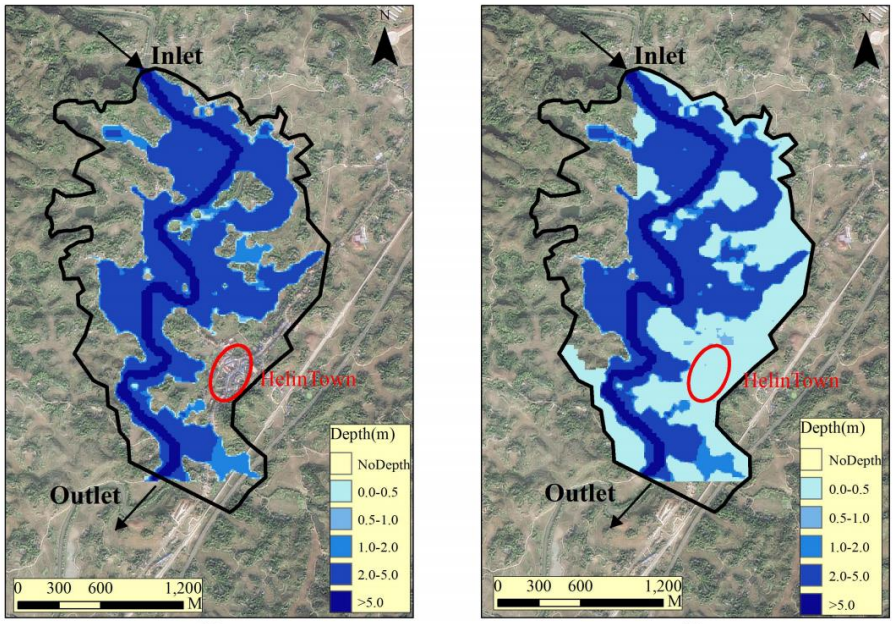

Figure 20. Comparison of maximum depth, (a)case A, (b)case C. Red circle denotes location of Helin town(Satellite imagery base map was obtain from Google Earth)

The capability of DBCM for switching models dynamically during computational process is tested, and the parameters of water depth, velocity and flux term are selected to conduct this assessment. The water depth threshold (0.01m) is used to distinguish the two models. Velocity is calculated in all of the inundation region, while the flux term is computed only in the region where hydrodynamic model is used, not the hydrologic model region. As shown in Fig.23, the rainfall stopped after 17h since the simulation started, and the surface flow on the slope gradually decreases. Flux calculation no longer exists in most part of the slope regions. However, a small amount of water is still left on the sloping area, and the flow in the confluence area is calculated by the hydrologic model (DWE). Thus, even though flux calculation has stopped, flow velocity still exists in most of the slope. The low-lying area at the northeast corner, due to the obstruction of the terrain, cannot be flooded in Case A. However, through the DBCM, the confluence of the surrounding slope accumulated to the local area and form a small range of flooded area.

Fig.22 shows the evolvement of coupling boundary of DBCM in Case B. In the early 8h, rainfall intensity is small (see Fig.19), and most of the runoff were infiltrated. Thus, the surface flow were determined by SWE with the upstream inflow. After that, rainfall begins to increase, and runoff start to generate surface flow using DWE. The region of SWE continues to extend until the inundation area reach a maximum value. And then, the area begins to shrink with the decreasing of rainfall.

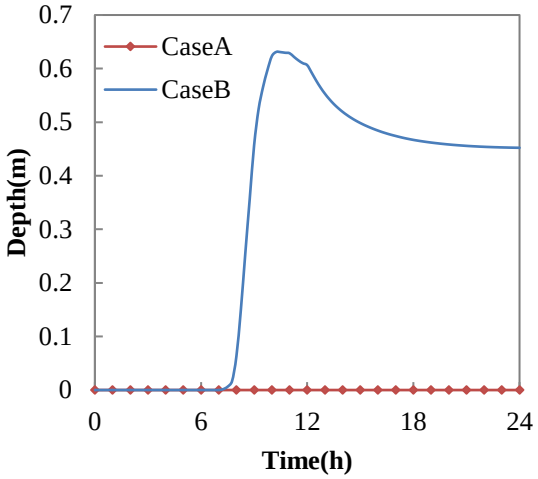

475

Figure 21. Comparison of water depth variation

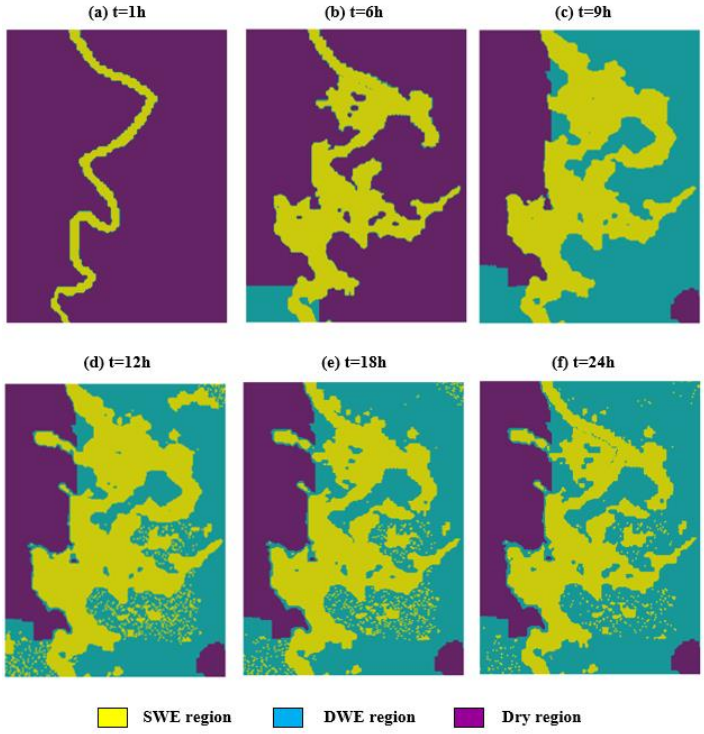

Figure 22 Evolvement of coupling boundary

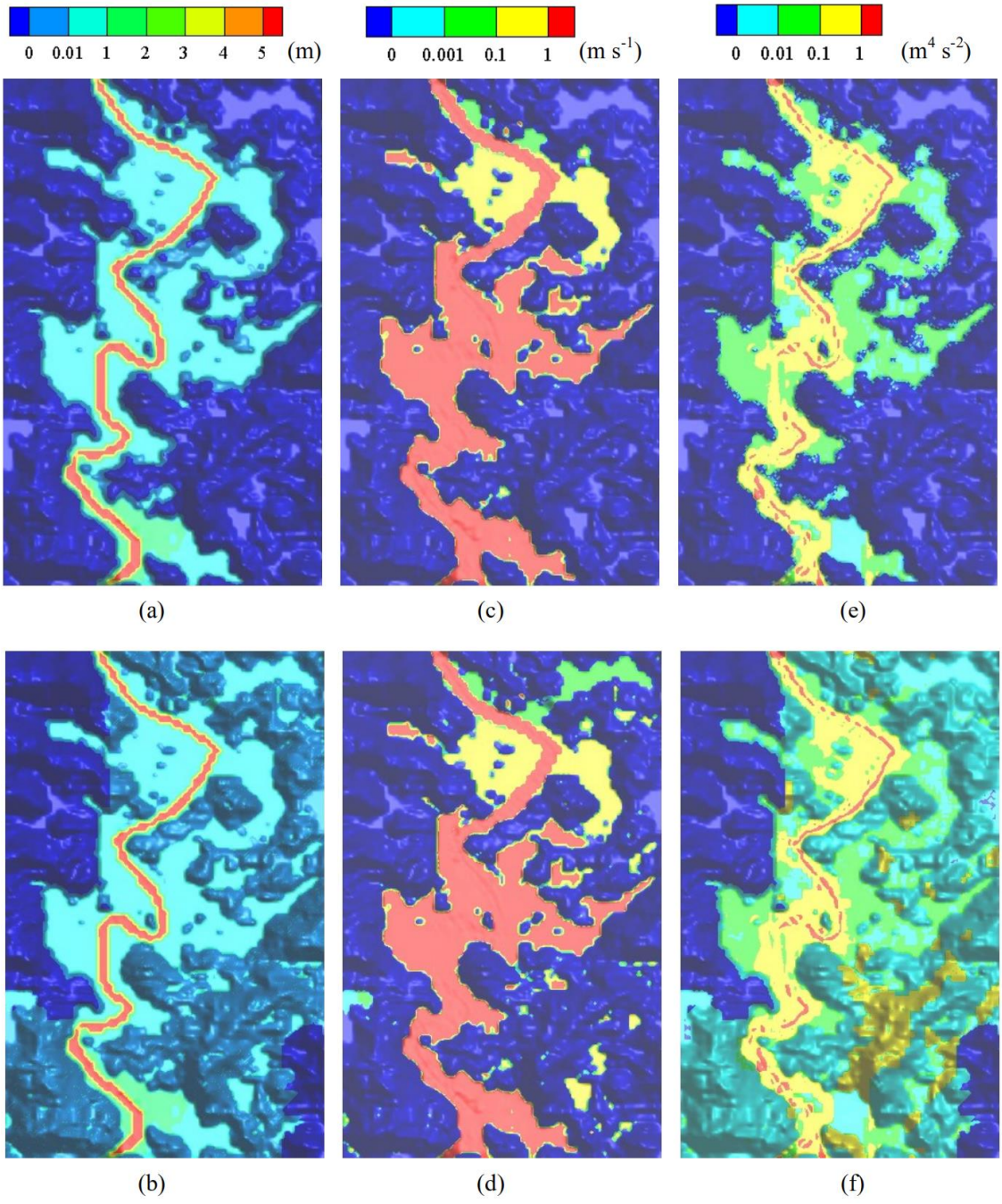

Figure 23. Simulation results at t=17h, (a) and (b) are water depth(m) for case A and case C,(c) and (d) are velocity(m s^{-1}) for case A and case C, (e) and (f) are flux term(m^4 s^{-2}) for case A and case C

5 Conclusions

A dynamic bidirectional coupling model (DBCM) for surface flow inundation simulation was developed. The mathematical formulations and solution scheme of the DBCM are realized. In DBCM, the runoff production is depicted by the hydrologic model through the rainfall-runoff process, while the hydrodynamic model emphasizes on the flood propagation processes. The characteristic wave theory is applied to determine the coupling boundary between the hydrologic and hydrodynamic computational domains.

In using the proposed DBCM, a dynamic alteration of the boundary position is realized for determining the non-inundation and inundation regions, which accounts the mass and momentum exchange and interaction between the two regions. The hydrologic and hydrodynamic model are carried out simultaneously. The DBCM is more in line with the natural physical process of flood formation and propagation, which has the potential to improve the accuracy of flood prediction.

The main advantage of the proposed DBCM are:(1) Based on the characteristic speed theory to predict flow propagation. The DBCM realizes the discharge calculation at coupling boundary by coupling slope gradient analysis and characteristic wave analysis, which are the foundations for solving hydrologic model and hydrodynamic model respectively. (2) The discharge on coupling boundary is used to update conservation variables of hydrologic model and hydrodynamic model with explicit physical significance based on the consideration of the flow information on both sides of the coupling boundary.(3) Contrast with the UCM and BCM, where the computational domains for hydrologic and hydrodynamic models are independent of each other and remain fixed, the DBCM can resize the computational domains of inundation and non-inundation regions according to the flow state throughout the calculation process, which is more aligned with natural rainfall and flood propagation conditions.

Three benchmark tests show that the DBCM is capable of accurately simulating the hydrologic and hydrodynamic response to rainfall events in various catchments. The DBCM gains good agreement with the analytical solution, and realizes the dynamic switching between the hydrologic and hydrodynamic models in simulating surface flow, which hardly achieved by former methods with single model working. The DBCM also succeeds in predicting the inundation regions in real flood events with more reasonable results when compared with the UCM.

Data availability

Model simulation and calibration data are available upon request from the corresponding author. Digital elevation model data are provided by the Geospatial Data Cloud at http://www.gscloud.cn. The data sets of Soil Properties and Land cover are provided by Cold and Arid Regions Sciences Data Center at Lanzhou (http://westdc.westgis.ac.cn). The Satellite imagery base map of Helin town was obtained from Google earth Pro.

Author contributions

YWY designed the methodology and carried out the investigation with cooperation from all co-authors. QZ provided the original model input data. The study was supervised by CBJ. YWY prepared the first draft of the manuscript, which was then revised and improved by the co-authors.

Competing interests

The authors declare that they have no conflict of interest.

Acknowledgements

This study was supported by the National Science Foundation of China (No. 51679121) and National Key Research and Development Program of China(NO. 2016YFC0502204).

References

References:

Ata, R., Pavan, S., Khelladi, S. and Toro, E.F.: A Weighted Average Flux (WAF) scheme applied to shallow water equations for real-life applications, Advances in Water Resources, 62, 155-172, 10.1016/j.advwatres.2013.09.019, 2013.

Bates, P.D. and De Roo, A.P.J.: A simple raster-based model for flood inundation simulation, Journal of Hydrology, 236, 54-77, https://doi.org/10.1016/S0022-1694(00)00278-X, 2000.

Borah, D.K. and Bera, M.: Hydrologic modeling of the Court Creek watershed, 2000.

Bouilloud, L. et al.: Coupling the ISBA Land Surface Model and the TOPMODEL Hydrological Model for Mediterranean Flash-Flood Forecasting: Description, Calibration, and Validation, Journal of Hydrometeorology, 11, 315-333, 10.1175/2009JHM1163.1, 2010.

Bradbrook, K.: JFLOW: a multiscale two-dimensional dynamic flood model, Water and Environment Journal, 20, 79-86, 10.1111/j.1747-6593.2005.00011.x, 2006.

Bradbrook, K.F., Lane, S.N., Waller, S.G. and Bates, P.D.: Two dimensional diffusion wave modelling of flood inundation using a simplified channel representation, International Journal of River Basin Management, 2, 211-223, 10.1080/15715124.2004.9635233, 2004.

Bravo, J.M., Allasia, D., Paz, A.R., Collischonn, W. and Tucci, C.E.M.: Coupled Hydrologic-Hydraulic Modeling of the Upper Paraguay River Basin, Journal of Hydrologic Engineering, 17, 635-646, 10.1061/(ASCE)HE.1943-5584.0000494, 2012.

Chen, A.S., Evans, B., Djordjević, S. and Savić, D.A.: A coarse-grid approach to representing building blockage effects in 2D urban flood modelling, Journal of Hydrology, 426-427, 1-16, https://doi.org/10.1016/j.jhydrol.2012.01.007, 2012.

Choi, C.C. and Mantilla, R.: Development and Analysis of GIS Tools for the Automatic Implementation of 1D Hydraulic Models Coupled with Distributed Hydrological Models, Journal of Hydrologic Engineering, 20, 06015005, 10.1061/(ASCE)HE.1943-5584.0001202, 2015.

Di Baldassarre, G., Giammarco, P., Todini, E. and Lamberti, P.: A conservative finite elements approach to overland flow: the control volume finite element formulation, Journal of Hydrology, 175, 267-291, 10.1016/S0022-1694(96)80014-X, 1996.

Downer, C.W., Ogden, F.L., Martin, W.D. and Harmon, R.S.: Theory, development, and applicability of the surface water hydrologic model CASC2D, Hydrological Processes, 16, 255-275, 10.1002/hyp.338, 2002.

Fraccarollo, L. and Toro, E.F.: Experimental and numerical assessment of the shallow water model for two-dimensional dam-break type problems, Journal of hydraulic research, 33, 843-864, 10.1080/00221689509498555, 1995.

Godunov, S.K.: A finite difference method for the computation of discontinuous solutions of the equations of fluid dynamics, Sbornik: Mathematics, 47, 357-393, 1959.

Grimaldi, S., Petroselli, A., Arcangeletti, E. and Nardi, F.: Flood mapping in ungauged basins using fully continuous hydrologic–hydraulic modeling, Journal of Hydrology, 487, 39-47, 10.1016/j.jhydrol.2013.02.023, 2013.

Hdeib, R., Abdallah, C., Colin, F., Brocca, L. and Moussa, R.: Constraining coupled hydrological-hydraulic flood model by past storm events and post-event measurements in data-sparse regions, Journal of Hydrology, 565, 160-176, 10.1016/j.jhydrol.2018.08.008, 2018.

Hsu, M.H., Chen, S.H. and Chang, T.J.: Inundation simulation for urban drainage basin with storm sewer system, Journal of Hydrology, 234, 21-37, https://doi.org/10.1016/S0022-1694(00)00237-7, 2000.

Laganier, O., Ayral, P.A., Salze, D. and Sauvagnargues, S.: A coupling of hydrologic and hydraulic models appropriate for the fast floods of the Gardon River basin (France), Nat. Hazards Earth Syst. Sci., 14, 2899-2920, 10.5194/nhess-14-2899-2014, 2014.

Leandro, J., Chen, A.S. and Schumann, A.: A 2D parallel diffusive wave model for floodplain inundation with variable time step (P-DWave), Journal of Hydrology, 517, 250-259, 10.1016/j.jhydrol.2014.05.020, 2014.

Lerat, J., Perrin, C., Andréassian, V., Loumagne, C. and Ribstein, P.: Towards robust methods to couple lumped rainfall--runoff models and hydraulic models: A sensitivity analysis on the Illinois River, Journal of Hydrology, 123-135, 10.1016/j.jhydrol.2009.09.019, 2012.

Li, D., Bou-Zeid, E., Baeck, M.L., Jessup, S. and Smith, J.A.: Modeling Land Surface Processes and Heavy Rainfall in Urban Environments: Sensitivity to Urban Surface Representations, Journal of Hydrometeorology, 14, 1098-1118, 10.1175/JHM-D-12-0154.1, 2013.

Li, D., Malyshev, S. and Shevliakova, E.: Exploring historical and future urban climate in the Earth System Modeling framework: 1. Model development and evaluation, Journal of Advances in Modeling Earth Systems, 8, 917-935, 10.1002/2015MS000578, 2016.

Liang, D., Lin, B. and Falconer, R.A.: Simulation of rapidly varying flow using an efficient TVD–MacCormack scheme, International journal for numerical methods in fluids, 53, 811-826, 2007.

Liu, G., Schwartz, F.W., Tseng, K. and Shum, C.K.: Discharge and water-depth estimates for ungauged rivers: Combining hydrologic, hydraulic, and inverse modeling with stage and water-area measurements from satellites, Water Resources Research, 51, 6017-6035, 10.1002/2015WR016971, 2015.

McMillan, H.K. and Brasington, J.: End-to-end flood risk assessment: A coupled model cascade with uncertainty estimation, Water Resources Research, 44, 10.1029/2007WR005995, 2008.

Montanari, M. et al.: Calibration and sequential updating of a coupled hydrologic-hydraulic model using remote sensing-derived water stages, Hydrology and Earth System Sciences, 13, 367-380, 10.5194/hess-13-367-2009, 2009.

Osti, R.P.: Strengthening Flood Risk Management Policy and Practice in the People's Republic of China: Lessons Learned from the 2016 Yangtze River Floods, 2017.

Panday, S. and Huyakorn, P.S.: A fully coupled physically-based spatially-distributed model for evaluating surface/subsurface flow, Advances in water Resources, 27, 361-382, 10.1016/j.advwatres.2004.02.016, 2004.

Patro, S., Chatterjee, C., Mohanty, S., Singh, R. and Raghuwanshi, N.S.: Flood inundation modeling using MIKE FLOOD and remote sensing data, Journal of the Indian Society of Remote Sensing, 37, 107-118, 10.1007/s12524-009-0002-1, 2009.

Rallison, R.E. and Miller, N.: Past, present, and future SCS runoff procedure, Rainfall-runoff relationship/proceedings, International Symposium on Rainfall-Runoff Modeling held May 18-21, 1981 at Mississippi State University, Mississippi State, Mississippi, USA/edited by VP Singh, Littleton, Colo.: Water Resources Publications, c1982., 1982.

Rawls, W.J., Brakensiek, D.L. and Miller, N.: Green–ampt Infiltration Parameters from Soils Data, Journal of Hydraulic Engineering, 109, 62-70, 10.1061/(ASCE)0733-9429(1983)109:1(62), 1983.

Rayburg, S. and Thoms, M.: A coupled hydraulic–hydrologic modelling approach to deriving a water balance model for a complex floodplain wetland system, Hydrology Research, 40, 364-379, 10.2166/nh.2009.110, 2009.

Rogers, B., Fujihara, M. and Borthwick, A.G.: Adaptive Q–tree Godunov–type scheme for shallow water equations, International Journal for Numerical Methods in Fluids, 35, 247-280, 10.1002/1097-0363(20010215)35:3<247::AID-FLD89>3.0.CO;2-E, 2001.

Singh, J., Altinakar, M.S. and Ding, Y.: Numerical Modeling of Rainfall-Generated Overland Flow Using Nonlinear Shallow-Water Equations, Journal of Hydrologic Engineering, 20, 04014089, 10.1061/(ASCE)HE.1943-5584.0001124, 2015.

Singh, V.P. and Woolhiser, D.A.: Mathematical Modeling of Watershed Hydrology, Journal of hydrologic engineering, 4, 270-292, 10.1061/(ASCE)1084-0699(2002)7:4(270), 2002.

Thompson, J.R.: Simulation of Wetland Water-Level Manipulation Using Coupled Hydrological/Hydraulic Modeling, Physical Geography, 25, 39-67, 10.2747/0272-3646.25.1.39, 2004.

Thompson, J.R., Sørenson, H.R., Gavin, H. and Refsgaard, A.: Application of the coupled MIKE SHE/MIKE 11 modelling system to a lowland wet grassland in southeast England, Journal of Hydrology, 293, 151-179, 2004.

Toro, E.F., Shock-capturing methods for free-surface shallow flows, John Wiley, 2001.

Viero, D.P., Peruzzo, P., Carniello, L. and Defina, A.: Integrated mathematical modeling of hydrological and hydrodynamic response to rainfall events in rural lowland catchments, Water Resources Research, 50, 5941-5957, 10.1002/2013WR014293, 2014.

Yu, C. and Duan, J.: Two-Dimensional Hydrodynamic Model for Surface-Flow Routing, Journal of Hydraulic Engineering, 140, 04014045, 10.1061/(ASCE)HY.1943-7900.0000913, 2014.

Yu, C. and Duan, J.: Simulation of Surface Runoff Using Hydrodynamic Model, Journal of Hydrologic Engineering, 22, 04017006, 10.1061/(ASCE)HE.1943-5584.0001497, 2017.

Yu, C. and Duan, J.G.: High resolution numerical schemes for solving kinematic wave equation, Journal of Hydrology, 519, 823-832, 10.1016/j.jhydrol.2014.08.003, 2014.

Yu, D. and Lane, S.N.: Urban fluvial flood modelling using a two‐dimensional diffusion‐wave treatment, part 1: mesh resolution effects, Hydrological Processes, 20, 1541-1565, 10.1002/hyp.5935, 2006.

Zhu, Z. et al.: Integrated urban hydrologic and hydraulic modelling in Chicago, Illinois, Environmental Modelling & Software, 77, 63-70, 10.1016/j.envsoft.2015.11.014, 2016.